International Journal of Solids and Structures 46 (2009) 4192–4207

Contents lists available at ScienceDirect

International Journal of Solids and Structures

journal homepage: www.elsevier.com/locate/ijsolstr

An experimental and computational study of laminated paperboard creasing and folding

L.A.A. Beex, R.H.J. Peerlings *

Department of Mechanical Engineering, Eindhoven University of Technology, P.O. Box 513, 5600 MB Eindhoven, The Netherlands

ARTICLE INFO

Article history:
Received 9 January 2009
Received in revised form 9 July 2009
Available online 25 August 2009

Keywords:
Paperboard
Creasing
Folding
Experimental mechanics
Numerical simulation
Finite element method
Delamination
Plasticity

ABSTRACT

Laminated paperboard is often used as a packaging material for products such as toys, tea and frozenfoods. To make the paperboard packages appealing for consumers, the fold lines must be both neat and undamaged. The quality of the folds depends on two converting processes: the manufacture of fold lines (creasing) and the subsequent folding. A good crease contains some delamination, initiated during creasing, to reduce the bending stiffness and to prevent the board from breaking during folding. However, for boards of high grammage breaking of the top layer is nevertheless a frequent problem. The mechanisms that operate in the creasing zone during creasing and folding, and that may thus result in breaking of the top layer, are studied in this contribution on the basis of idealized small-scale creasing and folding experiments. However, since experimental observations are only limited means to study the paperboard's behavior, a mechanical model is proposed to obtain more detailed insight. Although the material and delamination descriptions used in the mechanical model are both relatively straightforward, comparisons between the model and the experimental data show that the model predicts the paperboard's response well. The mechanical model shows – in combination with experimental strain fields – that multiple delaminations are initiated in the shear regions. Moreover, only the mechanical model reveals the mechanism that is responsible for the failure of the top layer if a crease is too shallow. Finally, the model also demonstrates that not only delamination but also plastic behavior must occur during creasing if breaking of the top layer is to be avoided.

1. Introduction

Laminated paperboard is a widely used packaging material. Its use is increasing every year, mostly because it is almost 100% recyclable and inexpensive. Paperboard can be converted into packages by relatively straightforward operations such as cutting, folding and glueing. However, a difficulty in paperboard converting is the cracking of boards of high grammage during folding. Cracked folds render packages less appealing to consumers and also compromise their strength.

The quality of folds and the likelihood of cracking depend on the previous definition of fold lines by creasing (or scoring). Both processes must therefore be taken into account in studying folding with a view to preventing cracking. In practice, both are optimized using empirical knowledge, but systematic studies of the mechanics underlying both processes – particularly cracking – are scarce. Nagasawa et al. (2003) investigated the influence of different creasing settings on the subsequent folding response in an experimental parameter study. They have shown that the maximum bending moment during folding depends on the nominal shearing strain that occurs during creasing. Computational models for creasing and folding were proposed by Xia et al. (2002) and Choi et al. (2007). The model proposed by Xia et al. (2002) uses a complex and detailed material and delamination model. The material description is orthotropic; the principal directions are given by the machine direction (MD), cross-fiber-direction (CD) and thickness direction (ZD). The delamination description differentiates between normal and tangential opening behavior, and allows the latter to be dependent of the normal compression.

The mechanical model of Choi et al. (2007) uses a material description that combines the Ramberg–Osgood model (Ramberg and Osgood, 1943) and the model of Karafillis and Boyce (1993) as proposed earlier by Mäkelä and Östlund (2003). Choi et al. (2007) extended this description with a non-linear elastic response in ZD. It is unclear how delamination is incorporated in their model. The model is qualitatively validated using experimental creasing strain fields.

In other studies, that are not directly related to laminated paperboard creasing, material models for paper have been proposed by Stenberg (2003) for the out-of-plane behavior and by Sawyer et al. (1998) and Castro and Ostoja-Starzewski (2003) for the in-plane behavior. Damage-based material descriptions for paper were developed in the studies of Isaksson et al. (2004) and

* Corresponding author. Tel.: +31 40 247 2788; fax: +31 40 244 7355.
E-mail address: r.h.j.peerlings@tue.nl (R.H.J. Peerlings).

0020-7683/$ - see front matter © 2009 Elsevier Ltd. All rights reserved.
doi:10.1016/j.ijsolstr.2009.08.012

Isaksson and Hägglund (2005). Moreover, Isaksson and Hägglund (2005) use the crack tip energy release rate as a failure criterion for delamination. Beldie (2001), Barbier et al. (2004) and Thakkar et al. (2008) used conventional Hill-plasticity to simulate the responses of both paperboard and corrugated board.

A study that reveals and explains the quintessential aspects of laminated paperboard's behavior in the creasing zone during creasing and folding and captures them in a model of limited complexity, seems to be missing. Our study tries to fill this gap by proposing a finite element (FE) model of three-layered paperboard that describes paperboard's behavior during creasing and folding. The FE model is based on experimental observations obtained using a lab-scale creasing and folding tool. It includes a continuum model to describe the material behavior of paper while a delamination model describes the opening behavior between different paper plies. The material and delamination model are both fairly straightforward so as to keep the model simple, which in turn minimizes the experimental parameter identification. All material and delamination parameters were separately determined for every paper layer in independent experiments. This ensures that the numerical simulations using the model are accurate predictions. Consequently, the model cannot only be used to explain the mechanisms within paperboard as observed in the creasing and folding experiments, but it can also be used to predict the paperboard's response for different creasing settings. The model was quantitatively validated by the use of: (1) experimental strain fields and force–crease depth curves during creasing and (2) moment–angle curves during folding. The behavior of paperboard during the creasing and folding processes is discussed in detail, and finally the mechanism responsible for breaking of the top layer is revealed for shallow creasing.

The structure of this paper is as follows. Section 2 discusses the setup used in the small-scale creasing and folding experiments on which the model is based, as well as preliminary observations made during the experiments. The mechanical model including the material model and delamination model are described in Section 3. Experimental and numerical results of creasing and folding are presented and compared in Section 4. Finally, conclusions of our study are presented in Section 5.

2. Creasing and folding experiments

2.1. Experimental setup

The purpose of the creasing and folding experiments is to discover general mechanisms and to provide a reference for comparison with predictions of the mechanical model. A miniaturized experimental tool has been developed which allows us to define a single fold line by creasing and subsequently folding the board sample along the crease. Because most problems with breaking of top layers occur if the creasing rule is placed parallel to the CD, this situation is taken in the experiments.

Fig. 1 is a schematic representation of the experimental tool. The samples are cut out of paperboard sheets which were kindly provided by Mayr-Melnhof Eerbeek. They have a thickness of 900 μm and consist of a bottom layer of 50 μm thickness, a midlayer of 800 μm and a top layer of 50 μm. The midlayer contains fresh-fiber mechanical pulp while the outer layers contain chemical pulp comprising a mixture of recycled and virgin fibers. The top layer is bleached to give a shiny appearance. The width of the samples in the direction of the creasing channel as shown in Fig. 1 is 20 mm, while the length of the samples perpendicular to the direction of the creasing channel is 28 mm. The width is sufficiently large to create plane strain conditions. Two holders are used to prevent the sample from moving upwards but not to clamp it horizontally. The distance between the holders is 20 mm. In the reference configuration, the creasing rule has a thickness of 1.05 mm and a radius equal to half its thickness. The standard crease depth is 900 μm, which equals the sample thickness. The width and height of the creasing channel are 2.50 and 1.00 mm, respectively. All parameters of the experimental tool can be varied to some extent but only the crease depth and the width of the creasing channel were changed in this study. A photograph of the creasing setup is shown on the left in Fig. 2.

A four-point-bending test is used to characterize the folding behavior (see Figs. 1 and 2). This test has the advantage that it is insensitive to inaccurate placement of the crease, because the bending moment does not vary between the two inner supports. All supports have a diameter of 1.00 mm and the distance between the centers of the outer supports is 16 mm; the distance between the centers of the inner supports is 6 mm. During preliminary folding tests, it became clear that the supports may indent the board samples. To prevent this, the folding tests are performed with pieces of thin aluminum foil placed between the samples and the supports (see Fig. 1).

The creasing and folding tools are mounted in a tensile stage which is used to determine force–displacement curves (see Fig. 2). These curves can provide much data, such as initial stiffness and energy dissipation, which can also be used for characterization and validation purposes. The tensile stage is sufficiently small to be placed under a light microscope so that the paperboard's behavior can be visualized during both processes. Strain fields during creasing are computed by digital image correlation (DIC).

The velocity of the creasing rule equals 5 μm/s and the relative velocity of the supports of the four-point-bending apparatus equals 40 μm/s. The experiments reported here were performed at a slightly fluctuating temperature and relative humidity of 21–23 °C and 15–30%, respectively.

2.2. Qualitative experimental observations

Microscopic images of samples that have been creased and folded are shown in Fig 3. They lead to two general observations which are important for constructing a mechanical model.

First, plastic deformation can be clearly observed in the creasing zone after both experiments. The remaining plastic strains after creasing could not be characterized by the use of DIC due to large local deformations. The plastic strain in ZD below the creasing rule after creasing is estimated at about −5%. The particular shape of the creasing zone after creasing is not caused by plastic strains in ZD but by out-of-plane shear strains and tensile strains in MD.

Secondly, the microscopic image obtained after folding shows that the midlayer has been separated from the outer layers – particularly from the top layer. The midlayer itself has been split up into several paper plies. The lower plies have been bent inwards and they have buckled, resulting in the typical shape shown in Fig. 3. Although somewhat arbitrary, the number of plies is approximately eight. Similar delamination behavior is observed in the folding results of Nagasawa et al. (2003) for thinner paperboards, although the number of plies formed may differ in these results.

The experimental strain fields and force–crease depth curves recorded during creasing and moment–angle curves recorded during folding are presented and compared to the numerical results in Section 4.

During creasing, out-of-plane compressive strains occur below the creasing rule and above the edges of the creasing channel. Out-of-plane shear strains occur between the creasing rule and the edges of the creasing channel. No in-plane tensile strains outside the creasing zone were detected in the experiments, whereas Savolainen (1998) confirms that they are present during industrial creasing (as shown on the left of Fig. 4). The presence of such

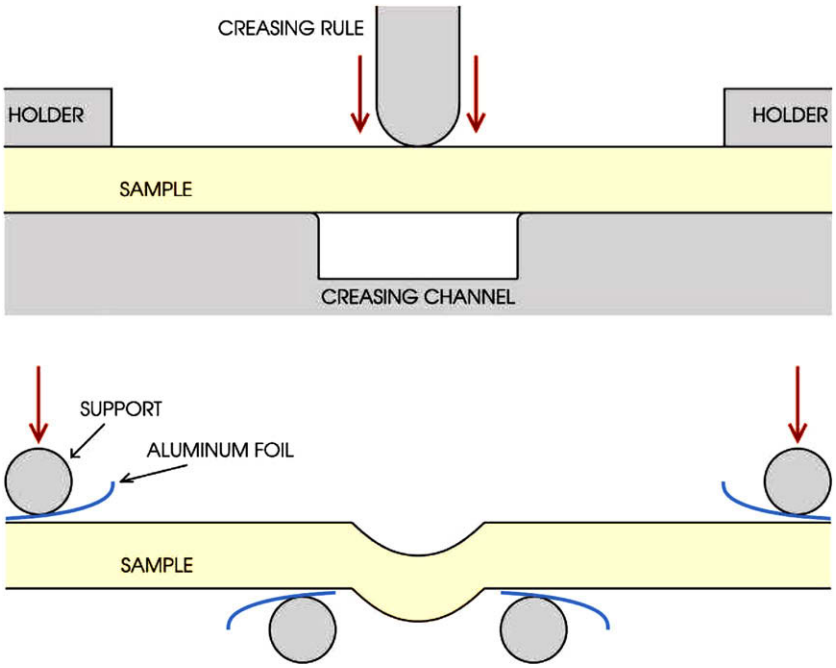

Fig. 1. Schematic representation of the board sample placed in the creasing tool (top) and in the folding tool after it has been creased (bottom).

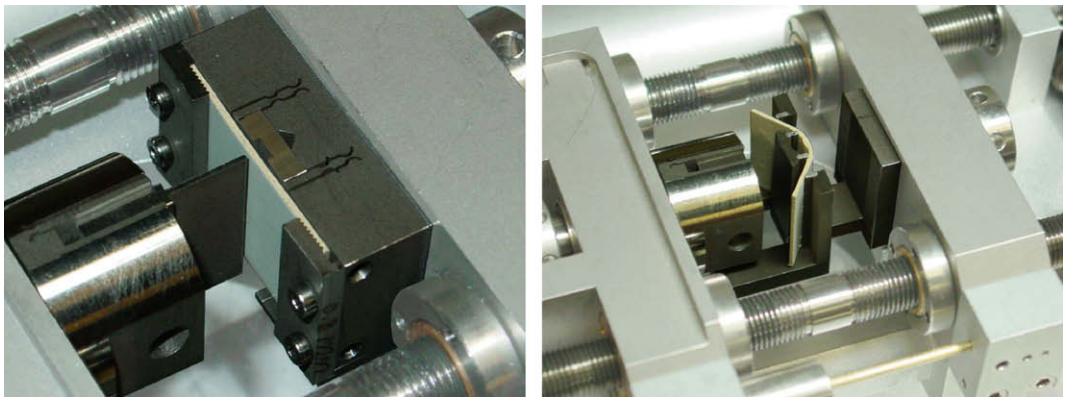

Fig. 2. The experimental tools mounted in the micro tensile stage; creasing setup (left) and folding setup (right).

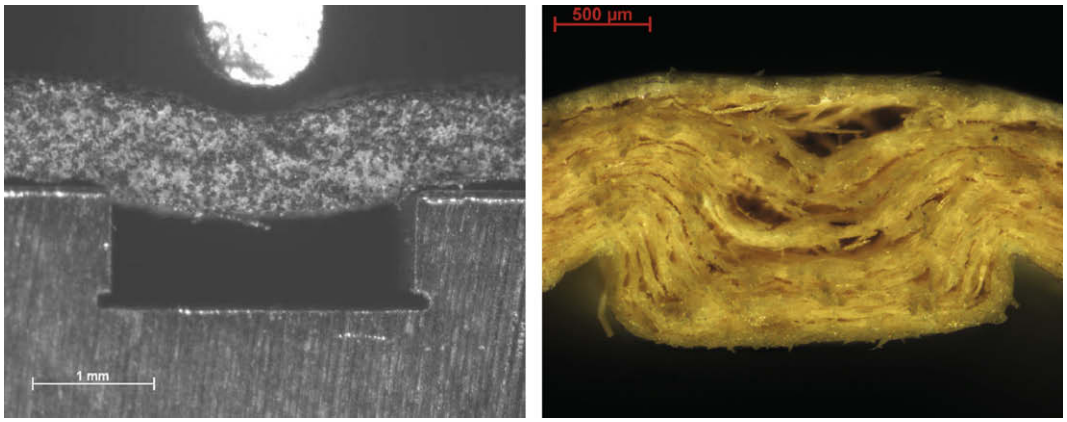

Fig. 3. (left) A board sample after creasing; a pattern has been applied to the sample to enable DIC. (right) The creasing zone of a sample after folding.

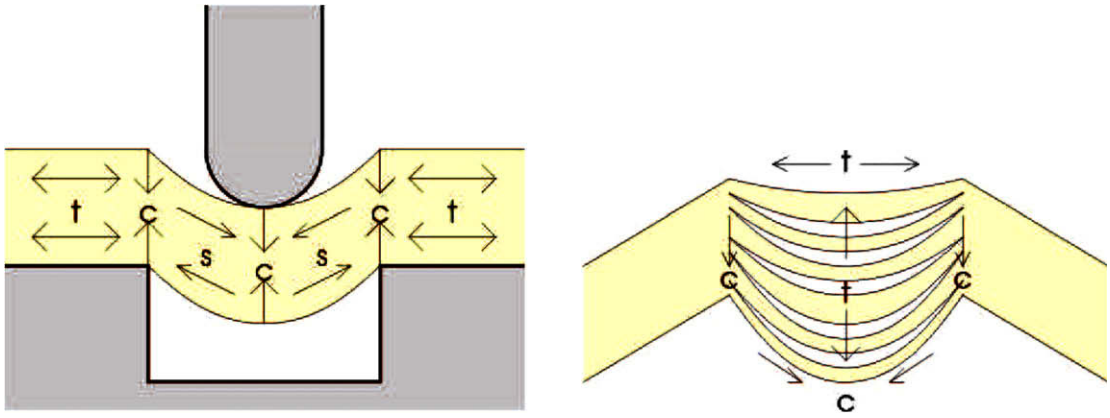

Fig. 4. Diagram of the deformation and stress state in the creasing zone during (left) creasing (Savolainen, 1998) and (right) folding; t, c and s represent tension, compression and shear, respectively.

strains depends on the level of constraint imposed on the board, which is rather low in our experiments due to the fact that the board is allowed to slide along the holders (see Section 2.1).

Separation of the midlayer into a number of thin paper plies and separation of the midlayer and the outer layers is present after folding (see the diagram on the right in Fig. 4). Savolainen (1998) and Xia (2002) report that this separation is initiated during creasing in the shear zones, but this was not directly detected in our experiments.

During folding, the lower plies can easily bend away due to the fact that they have a curved shape and are loaded in compression (see Fig. 4). Because the thin plies in the creasing zone are easier to bend than the paperboard outside the creasing zone, bending occurs solely in the creasing zone. At the same time, some out-of-plane tension may exist within the crease, due to fibers that bridge the (partially) delaminated surfaces. The upper plies, including the top layer, are loaded in in-plane tension which may cause the top layer to break. Therefore, creasing and folding must be performed in such a way that the in-plane loading of the top layer is kept to a minimum.

3. Finite element model

The purpose of the numerical model is to explain the experimental observations described in the previous section and to predict the behavior of paperboard for different creasing settings in a virtual environment. The model is constructed in such a way that it can easily be implemented in commercial finite element software. To render the model computationally efficient, a continuum model is used to describe the material behavior of paper, in combination with a delamination model so as to account for the opening behavior of different paper plies. Two crucial elements of the numerical model are therefore the elasto-plastic material model, which must accurately describe the material behavior of the different paper plies, and the delamination model which is used to describe opening behavior between the different plies. Both aspects are discussed in more detail below.

Fig. 5 is a schematic representation of the proposed model. This mechanical model can be used to describe the paperboard's behavior during creasing and subsequent folding. A two-dimensional model suffices, because plane strain conditions exist in the experiments. The tools have the same dimensions as in the experiments, and they are considered to be rigid and in frictionless contact with the board. Three layers of paper are distinguished in the mechanical model. Delamination surfaces are included within the thick middle layer and at the interfaces with the top and bottom layers; they are oriented parallel to the plane of the board and are assumed to show the same behavior. Initially the delamination surfaces are closed. Because delamination only occurs in the creasing zone, it suffices to model only the delamination surfaces in and around the creasing channel. However, they are sufficiently long to allow an arbitrary growth of the delamination in the lateral direction. Seven delamination surfaces are modeled across the thickness because this is the average number observed in the experiments. The mechanical model is relatively insensitive to small changes of the number of delamination surfaces. For a mechanical model with six delamination surfaces instead of seven the creasing and folding results only differ approximately 5%.

An FE model of the mechanical model was constructed in the MSC.Marc finite element software in which only one half of the mechanical model is needed due to symmetry. The paperboard is modeled with two-dimensional bi-linear plane strain elements, including assumed strain modes and a constant dilatation. Each ply, bounded by two delamination surfaces, is modeled with two elements over the thickness to save computational cost. The results of an FE simulation with four instead of two elements over the thickness of each ply show a difference of approximately 5%. The final mesh contains 3508 elements and 3731 nodes. An updated Lagrange approach was used for the incremental-iterative solution procedure and the convergence tolerance has been set to 0.1 in terms of relative residual forces.

3.1. Material model

The material model used by Beldie (2001), Barbier et al. (2004) and Thakkar et al. (2008) is used here for the individual layers because it is available in the software. Although this material model is comparatively simple and more advanced models exist (Xia et al., 2002; Stenberg, 2003; Castro and Ostoja-Starzewski, 2003; Isaksson et al., 2004), the aforementioned authors have shown that it can be used to describe the behavior of paper. Our results indicate that it also captures the essential mechanisms in paperboard creasing and folding and a more complex material model may therefore be unnecessary. The model takes into account the paperboard's orthotropic behavior, which is caused by the preferred direction of the fiber network. Moreover, the material model is elasto-plastic. The elastic behavior is linear and orthotropic, and Hill's yield criterion (Hill, 1950) is used to describe the onset of yield. Isotropic strain hardening is used. Although this means that the material description will not accurately take load reversal into account, the use of isotropic hardening keeps the experimental parameter identification to a minimum. The isotropic strain hardening is characterized by the following hardening function:

$$\sigma_y = \sigma_{y0}(1 + A\bar{\epsilon}_p)^m, \tag{1}$$

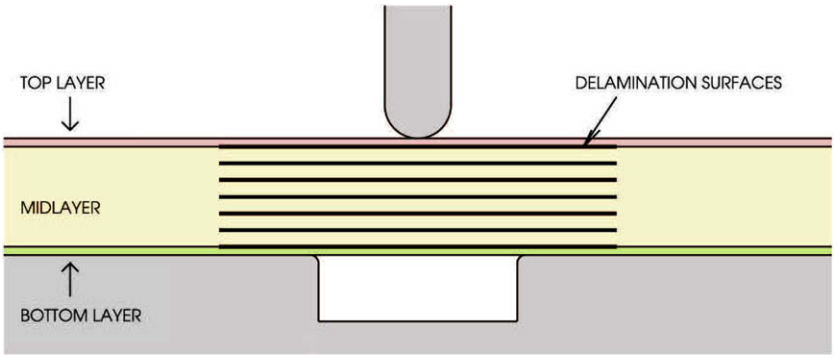

Fig. 5. Schematic representation of the mechanical model of creasing.

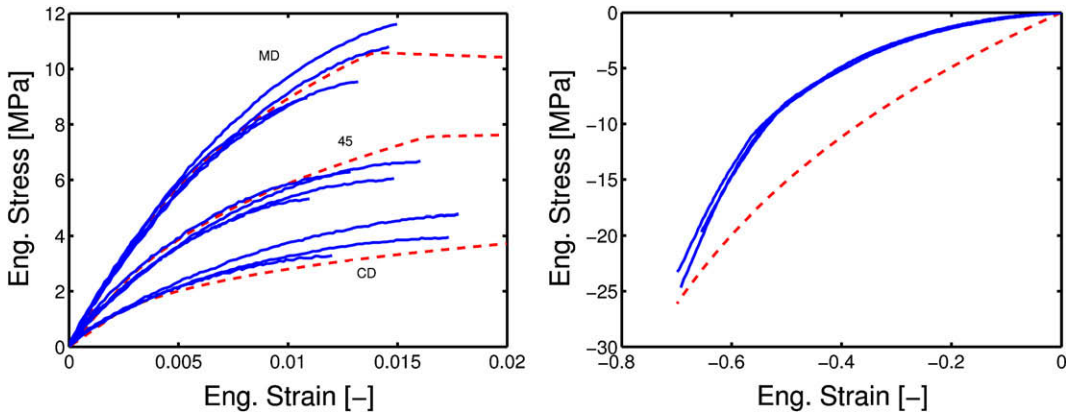

Fig. 6. Experimental results (solid) and fits (dashed) for the in-plane behavior (left) and out-of-plane behavior (right) of the midlayer.

where σ_{y0} is the initial reference yield stress, $\bar{\epsilon}_p$ is the equivalent plastic strain, and A and m are dimensionless hardening parameters. The same material description is used for the three different grades of paper that are present in the paperboard being considered, but the material parameters are determined separately for each material.

The material parameters are characterized in a similar manner to that used by Thakkar et al. (2008). In-plane tensile tests in MD, CD and at an angle of 45° were performed on the three paper layers to determine the in-plane material parameters. The responses thus obtained are compared with the experimental data in the diagram on the left in Fig. 6, and remain within the bandwidth of the experimental scatter. Out-of-plane compression and shear tests are only performed on the midlayer, as the other layers are too thin to carry out these tests properly. Sample dimensions of 5.0 mm × 5.0 mm × 0.80 mm and 10.0 mm × 5.0 mm × 0.80 mm have been used to confirm that the performed out-of-plane tests are size independent. In the out-of-plane compression tests a minor precompression is used to sufficiently hold the samples before performing the compression tests (see the left sketch in Fig. 7). In the out-of-plane shear tests a double-phase glue was used to fixate the sample to two metal strips. The double-phase glue is minimally absorbed by the midlayer and the average absorption depth was analyzed with microscopy so it can be accounted for. DIC has been used to verify that the samples are indeed strained in simple shear and the shear strain determined from the clamp displacement is indeed correct. The out-of-plane values for the outer layers are scaled according to the Young's moduli in MD. Because compression strains of over 55% are observed during creasing and the board shows a significant non-linearity over this range, the Young's modulus in ZD is taken as the secant stiffness measured for the midlayer (see the diagram on the right in Fig. 6).

Once the in-plane yield stresses have been set to a fixed value based on the in-plane tests, the yield stress in ZD can be set. To ensure that the yield surface is convex, the ZD yield stress must meet certain conditions (Hill, 1950; Beex, 2008). Due to these conditions and the relatively small Young's modulus in ZD, the out-of-plane compression response is dominated by elasticity. For this reason the ZD yield stress is of little influence on the ZD compression response and therefore the yield stress in ZD can be used to optimize the shape of the yield surface with respect to the in-plane plastic response. This has been achieved by assuming that the uniaxial stress response in MD – as measured in the tensile tests – should equal the plane strain response in MD – as used in the mechanical model. The condition that the apparent initial yield stress in both cases should be equal allows one to determine the corresponding out-of-plane yield stress $\sigma_{33,y}$ (Beex, 2008). The full set of material parameters used in the FE simulations is shown in Table 1.

3.2. Delamination model

The delamination surfaces are modeled by cohesive zones, which are nowadays commonly used for delamination (Xu and Needleman, 1993; Ortiz and Pandolfi, 1999; Chandra et al., 2002; Van den Bosch et al., 2007). The cohesive zone model of Ortiz and Pandolfi (1999) as implemented by Van Hal et al. (2007) has been used, in combination with a Coulomb friction model. The relatively simple cohesive zone model describes irreversible behavior in terms of damage, whereas the friction model gives rise to permanent deformation and accounts for an increasing maximum shear stress under increasing normal compression. In the cohesive zone model a different opening behavior in normal and tangential direction is obtained, depending on one parameter, which equals the ratio of the maximum tractions in both directions. The damage

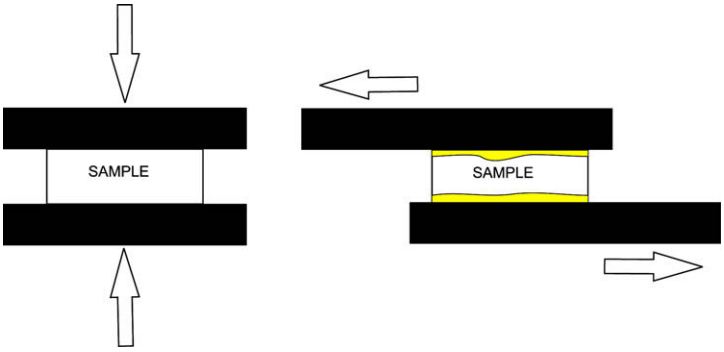

Fig. 7. Sketch of the out-of-plane compression test (left) and the out-of-plane shear test (right). Two small zones of the midlayer are influenced by the glue in the shear test.

Table 1
Material parameters determined by in-plane and out-of-plane tests as used in the numerical model. 1 indicates MD, 2 indicates CD and 3 indicates ZD.

	Midlayer	Top layer	Bottom layer
E_{11} [GPa]	1.31	3.52	1.87
E_{22} [GPa]	0.55	1.37	0.78
E_{33} [MPa]	22.3	60.0	31.9
G_{12} [GPa]	0.43	0.79	0.82
G_{13} [MPa]	13.5	13.5	13.5
G_{23} [MPa]	15.7	15.7	15.7
ν_{12} [–]	0.35	0.35	0.35
ν_{13} [–]	0.26	0.26	0.26
ν_{23} [–]	0.38	0.38	0.38
$\sigma_{11,y}$ [MPa]	3.67	19.8	16.0
$\sigma_{22,y}$ [MPa]	1.34	2.90	3.50
$\sigma_{33,y}$ [MPa]	1.36	3.34	3.58
$\sigma_{12,y}$ [MPa]	1.56	3.58	6.24
$\sigma_{13,y}$ [MPa]	2.12	11.4	9.24
$\sigma_{23,y}$ [MPa]	2.12	11.4	9.24
A [–]	5.70e3	1.21e3	0.74e3
m [–]	0.308	0.288	0.320

evolution law governs the traction–separation law and must thus be adapted to describe interfacial delamination in paperboard.

Cohesive zone formulations are characterized by two initially closed surfaces whose opening is governed by a traction vector and a separation vector. The traction and separation vectors are related to each other by a traction–separation law, which gives the necessary traction to obtain a certain separation of the surfaces. The magnitude and direction of the traction vector are dependent of the normal and tangential components of the separation. In this study the normal and shear components of the vectors are defined with respect to the average of the two material surfaces. In the cohesive zone formulation of Van Hal et al. (2007) an effective, scalar traction–separation (τ–λ) law is defined, the shape of which is governed by a damage evolution law. The effective separation λ is related to the normal and tangential separations according to the following equation:

$$\lambda = \sqrt{\langle \delta_n \rangle^2 + \beta^2 \delta_s^2}, \tag{2}$$

where the normal and tangential components of the separation vector are represented by δ_n and δ_s and the ratio between the maximum tangential traction $t_{s,max}$ and maximum normal traction $t_{n,max}$ is represented by $\beta = t_{s,max}/t_{n,max}$. The effective traction τ is the derivative of the cohesive energy Φ with respect to the effective separation λ:

$$\tau = \frac{\partial \Phi}{\partial \lambda}. \tag{3}$$

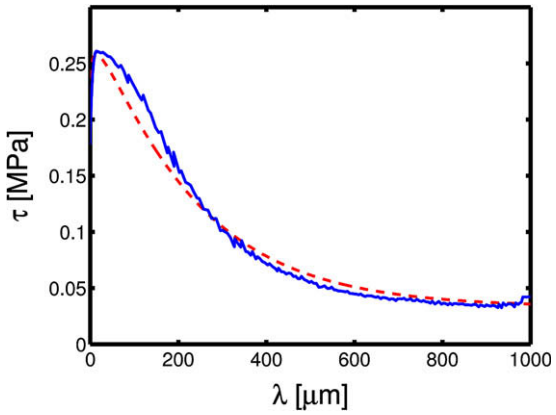

Fig. 8. Effective response of a single cohesive zone as obtained from the processed experimental shear data (solid) and the fitted traction–separation law (dashed).

The normal and tangential tractions, t_n and t_s, are derived using the rule of chains:

$$t_n = \frac{\partial \Phi}{\partial \delta_n} = \frac{\partial \Phi}{\partial \lambda}\frac{\partial \lambda}{\partial \delta_n} = \tau \frac{\langle \delta_n \rangle}{\lambda} \tag{4}$$

$$t_s = \frac{\partial \Phi}{\partial \delta_s} = \frac{\partial \Phi}{\partial \lambda}\frac{\partial \lambda}{\partial \delta_s} = \tau \beta^2 \frac{\delta_s}{\lambda}. \tag{5}$$

Once the effective traction–separation law $\tau(\lambda)$ has been determined, the combined opening and sliding response, for a given value β, are solely governed by Eqs. (2)–(5). The relation between the effective traction and effective separation is fitted to pure out-of-plane shear tests on the midlayer in MD because during creasing, delamination is initiated by shear stresses (Xia, 2002). The normal response – obtained by pure out-of-plane tensile experiments – is only used to determine the ratio between the maximum shear traction and the maximum normal traction, β. This introduces some degree of approximation for the opening response, whereas the sliding response is captured quite accurately – see ahead to Fig. 9. The raw shear data must be corrected to obtain the τ–λ relationship of one cohesive zone because in the mechanical model five cohesive zones are present in the midlayer (see Appendix A).

The final, averaged effective response of a single cohesive zone as extracted from the experiments is represented by the solid curve in Fig. 8. The following relation is proposed to capture this response:

$$\tau = \tau_\infty + (\tau_0 - \tau_\infty + B\lambda^\alpha) e^{\frac{-\lambda}{\lambda_\infty}}, \tag{6}$$

where

$$B = \frac{\lambda_{max}^{1-\alpha}}{\alpha \lambda_\infty} (\tau_{max} - \tau_\infty) e^{\frac{\lambda_{max}}{\lambda_\infty}}. \tag{7}$$

Table 2
Delamination parameters as used in the numerical model.

τ_0 [kPa]	178	Q_0 [μm]	0.1
λ_{max} [μm]	13.5	α [–]	0.167
τ_{max} [kPa]	263	β [–]	2.42
λ_∞ [μm]	207.5	μ [–]	1.10
τ_∞ [kPa]	33.1		

This relationship has also been plotted in Fig. 8. The initial traction at which damage starts to grow is τ_0 and τ_∞ is the final traction that remains at large opening displacements; the opening displacement at which the maximum traction τ_{max} occurs is denoted by λ_{max}. The parameter α is a measure for the steepness of the response before τ_{max} is reached and the parameter λ_∞ determines at which opening displacement τ_∞ is reached. In order to rephrase this traction–separation law in terms of a damage evolution law, we define Q_0 to be the separation at which damage starts to grow. The value of Q_0 is taken to be small so that the initial stiffness is very high ($K_0 = \tau_0/Q_0$). For effective openings beyond Q_0 the damage evolution law is defined such that upon substitution in the general traction–separation law

$$\tau = (1 - D)K_0\lambda \tag{8}$$

relation (6) results for monotonic loading.

Finally, out-of-plane shear tests under normal compression are performed to establish the friction coefficient μ in the friction model. The obtained delamination parameters for out-of-plane shear in MD are given in Table 2.

An FE model of the midlayer, including five cohesive surfaces, has been used to validate the delamination model in out-of-plane tension and shear. The results are shown Fig. 9. The numerical results stay within the scatter band of the experimental data for both loading directions. Unloading occurs according to the secant stiffness due to the use of the damage formulation. The influence of the friction model is not present in the shear results because no normal compression was applied.

4. Results

In this section, numerical results of the mechanical model described in Section 3 are compared to the experimental results for the reference case with standard creasing settings. The experimentally determined material parameters as presented in Section 3 are used in the mechanical model without any modification and the numerical results shown are therefore true predictions. Furthermore, the model is also validated for different channel widths and crease depths and the failure mechanism in case of small crease depths is established.

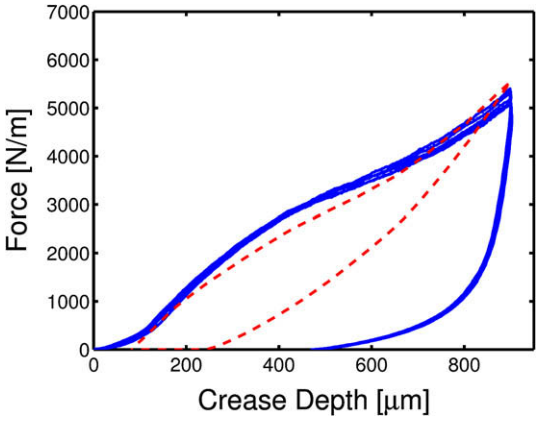

Fig. 10. The normalized force–crease depth curves obtained from the experiments (solid) and from the numerical analysis of the mechanical model (dashed).

4.1. Reference case: creasing

First the force–crease depth curve is considered to compare the model's response during creasing with that measured in the experiments. Fig. 10 clearly shows that the computed loading curve fits the experimental data well. Deviations are larger in the unloading response.

At small crease depths, below 100 μm, a non-linear response can be distinguished in the experimental results. This is caused by the fact the holders have some clearance because they are solely used to prevent the samples from moving upwards and not to clamp them. Moreover it is possible that the creasing rule is slightly mis-aligned, so that the creasing depth varies slightly over the width of the sample. This initial effect disappears at a crease depth of about 125 μm and it is not observed in the – idealized – simulations.

Ignoring the initial effect in the experimental data, we can distinguish three different stages during the loading phase of the creasing experiment. First, we see an initial response of which the experimental and computed stiffnesses are virtually identical. Subsequently, initiation of delamination occurs in the mechanical model at a crease depth of 200 μm and as a consequence the slope of the force–crease depth curve decreases. The delamination continues to grow until a crease depth of approximately 650 μm is reached. Around this point the creasing experiment essentially

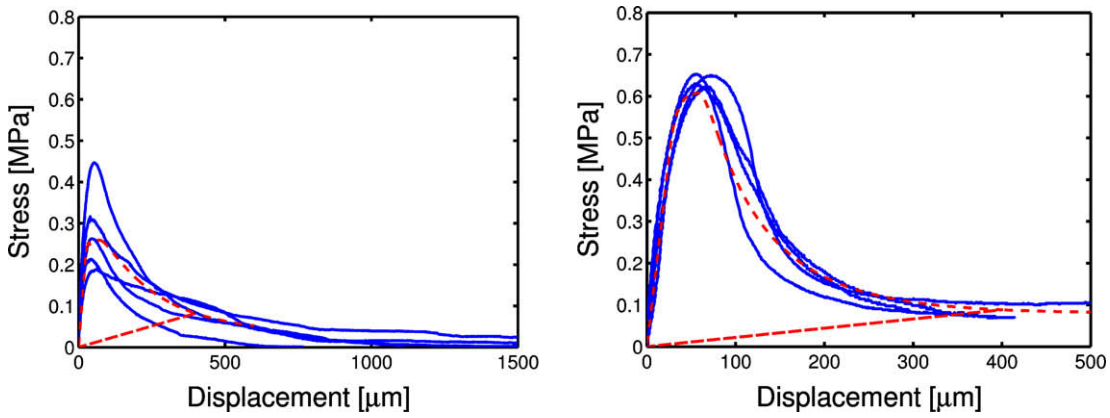

Fig. 9. The experimental results (solid) and the results of numerical simulations (dashed) of the out-of-plane tensile tests of the midlayer (left) and of the out-of-plane shear tests in MD of the midlayer (right).

turns into an out-of-plane compression test, which leads to an increasing slope of the force–crease depth response.

Although during the first phase of the creasing experiment the experimental and numerical stiffnesses are similar (see Fig. 10), the strain fields in Fig. 11 make clear that the mechanics which govern the initial deformation slightly differ between the experiment and the numerical simulation. In the experimental strain fields a disordered distribution of strains in MD can be distinguished while in the numerical result the shape of the MD strain fields implies some bending. Out-of-plane compressive strains are concentrated below the creasing rule and above the edge of the creasing channel and their magnitudes compare well. However, the compressive zone in the experiment is large above the edge of the creasing channel while in the numerical result this compressive region is smaller, which is consistent with the observation above that in the numerical simulation part of the response is governed by bending. This is caused by the fact that in this regime (compressive ZD strains $\leqslant 10\%$) the ZD stiffness is overestimated by the model – see Fig. 6. This high stiffness is also responsible for the relatively large out-of-plane shear zones in the numerical results. The shear zones grow during the creasing test but remain confined between the edges of the creasing rule and the creasing channel (see ahead to Fig. 12). Summarizing, we can say that the experiments show that the initial response is mostly governed by indentation. However, due to the high out-of-plane Young's modulus the numerical results show some shearing and bending as well.

In the second stage, delamination occurs in the zones where shear strains are observed in the experiments, as is confirmed by Savolainen (1998) and Xia (2002). This is made clear in Fig. 12

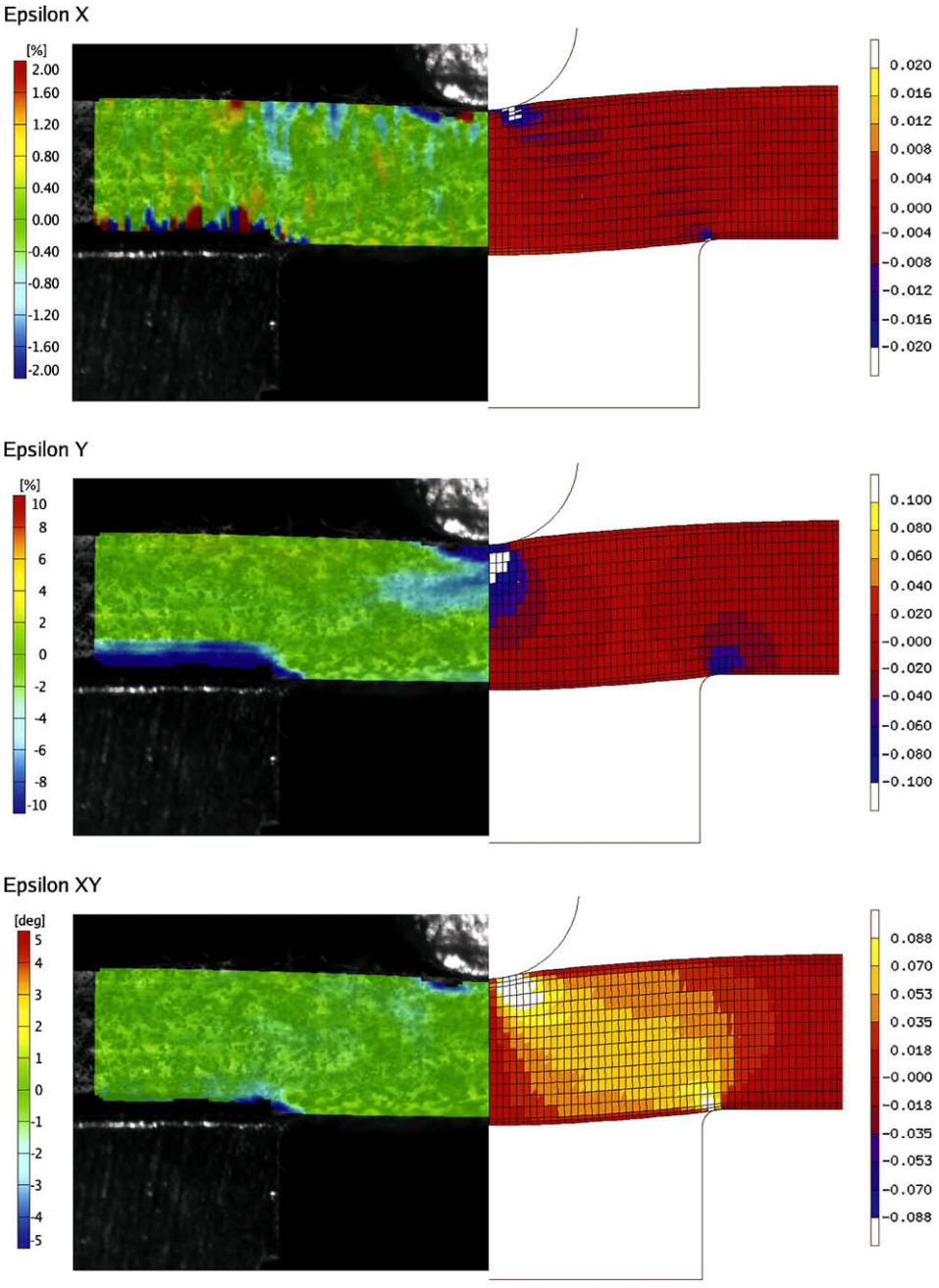

Fig. 11. Experimental (left) and numerical (right) strain fields at a crease depth of 141 μm: (top) the normal strain in MD, (middle) the out-of-plane (ZD) strain and (bottom) the out-of-plane shear strain in degrees in the experimental result (left) and in radians in the numerical result (right).

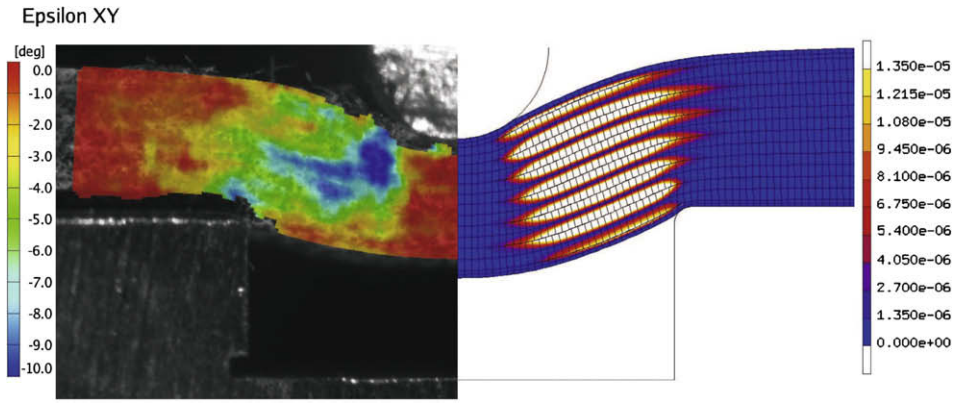

Fig. 12. (left) The experimental shear strain field at a crease depth of 542 μm and (right) the effective separation of the cohesive zones in the numerical model at the same crease depth. Blue/dark zones are still closed while white zones represent effective separations higher than 13.5 μm, which is the effective separation at which the maximum traction occurs.

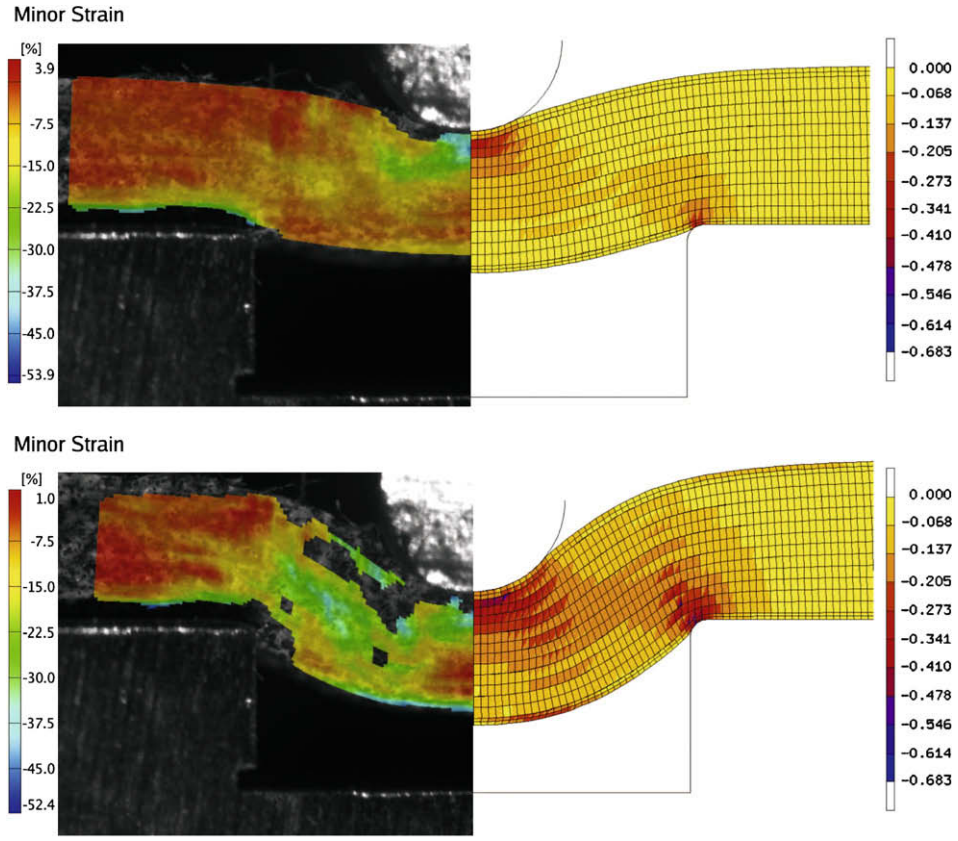

Fig. 13. Experimentally (left) and numerically (right) determined minor strains at a crease depth of 377 μm (top) and 753 μm (bottom).

where the experimental shear strains are plotted together with the numerically predicted separation of the delamination surfaces. The localization of the experimental shear strains may indicate delamination. Between the crease depths at which delamination is initiated and stops, the computed force is slightly lower than the experimental force (see Fig. 10). The cause may be that the delamination surfaces in the mechanical model are continuous and equally strong. As a result, all delamination surfaces in the midlayer become active at approximately the same crease depth and show the same opening behavior throughout the creasing process, see Fig. 12. Furthermore, the delaminated zones grow relatively rapidly along the straight, predefined cohesive zones. However, in actual paperboard delamination is initiated more randomly and does not follow straight planes. Delamination may therefore grow more gradually in the experiments and the measured force–crease depth curve deviates more slowly from the initial stiffness.

Another interesting observation in the numerical result of Fig. 12 is that more delamination is present in the midlayer than between the midlayer and the outer layers. A numerical analysis (not shown here) in which solely the creasing zone is loaded in pure out-of-plane shear shows that this is caused by edge effects. The midlayer is loaded more in shear than the outer layers due to the free edges of both outer layers.

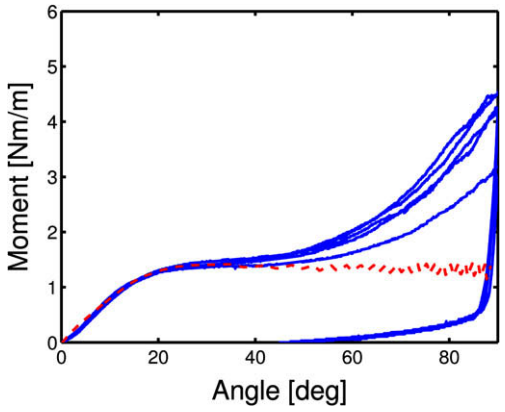

Fig. 14. The normalized moment–angle curves of the experiments (solid) and of the numerical analysis of the mechanical model (dashed).

Returning to the force–displacement response of Fig. 10, the mechanical model describes the increasing slope around 650 μm well, although the predicted slope is slightly too high. At this depth the creasing process starts to resemble a compression test because the delamination progress stops. This is shown for the experimental and simulation results in Fig. 13, where the minor strain represents out-of-plane compression. The fact that the predicted slope is slightly too high at this depth is again caused by the overestimated out-of-plane compressive stiffness at overall compression strains below 30% (see Fig. 6) as the response is essentially governed by compression of the board below the crease rule and on the edges of the crease channel.

In Fig. 13 compression strains are also clearly visible at the bottom of the creasing zone in the experimental strain fields. For this reason in-plane tension must be present at that location, which is most likely caused by friction between the sample and the creasing channel. Because friction between the tools and the sample is not taken into account in the mechanical model, this effect is not present in the numerical results.

The unloading behavior of the mechanical model does not match the experimental unloading (see Fig. 10). This is caused by the linear elastic modeling of the out-of-plane behavior. The unloading is essentially governed by the recovery of the through-thickness compressive strain. As the experimental compression response is essentially non-linear, it is poorly captured by the linear elasticity assumed here (see Fig. 6). The high linear stiffness in ZD also explains the difference in thickness reduction in the experimental and simulation results in Figs. 12 and 13.

4.2. Reference case: folding

After creasing, folding is performed by the use of the four-point-bending test. The moment–angle curve during folding is calculated from the force–displacement data of the micro tensile stage. The numerically established moment–angle curve is calculated in the same way. The computed moment–angle curve for the reference case is shown together with the experimental results in Fig. 14. The computed response matches the experimental data perfectly until an angle of approximately 40°. In the experiments it is observed that from this point onwards the aluminum foil makes contact with other parts of the experimental setup which leads to an increase of the moment–angle curve. No attempt has been made to take this effect into account in the mechanical model as it is an artifact of the experimental method used.

Three phases can be distinguished in the folding test. The response starts with an initial stiffness which is mainly determined by three mechanisms. They are illustrated by the computed shapes of the creasing zone after creasing and during the first part of the folding simulations as shown in Fig. 15. The top plies are loaded in in-plane tension, while the bottom plies bend inwards (downwards) due to the in-plane compression they experience. Due to the bending of the bottom plies and the in-plane tensile loading of the upper plies, the opening displacement of the delamination surfaces grows from the shear zones between the creasing rule and the side of the channel towards the middle of the creasing zone. When the maximum traction of the delamination surfaces is reached at the center, they can easily open in normal direction.

The second phase starts around 15°, when the slope of the moment–angle curve decreases. At this point, all delamination surfaces in the midlayer have reached the maximum traction of the cohesive zones, as is shown in the right picture in Fig. 15. Therefore, the cohesive zones barely contribute to the slope of the moment–angle curve anymore, which therefore decreases. Finally, a plateau is reached in the moment–angle curve at an angle of 25°. At this angle the top layer is oriented horizontally and only the bending of the lower plies contributes to the stiffness.

After 50° the numerical moment–angle curve oscillates due to the large rotation of the paperboard and the contact between the outer support and the relatively large elements which have been used near it. These oscillations therefore have no physical meaning.

The creasing zone predicted by the mechanical model at the end of the folding test is depicted in Fig. 16. Clearly the delamination surfaces in the midlayer show a large amount of opening displacement. The dilation between the upper plies within the midlayer is somewhat larger compared to the dilation in the lower plies. This trend can also be seen in the experimental results (see Fig. 3). The

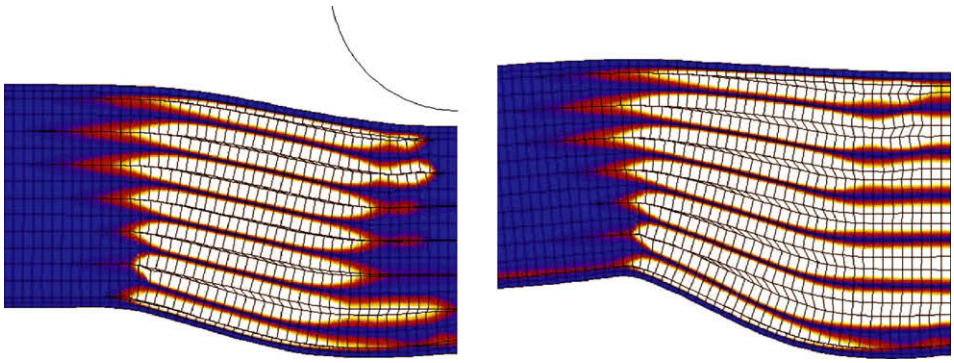

Fig. 15. (left) The creasing zone of the mechanical model after creasing. Blue zones are still closed while white zones represent effective separation beyond the traction peak. Plastic deformation is clearly present after creasing. (right) The creasing zone at a folding angle of 15°.

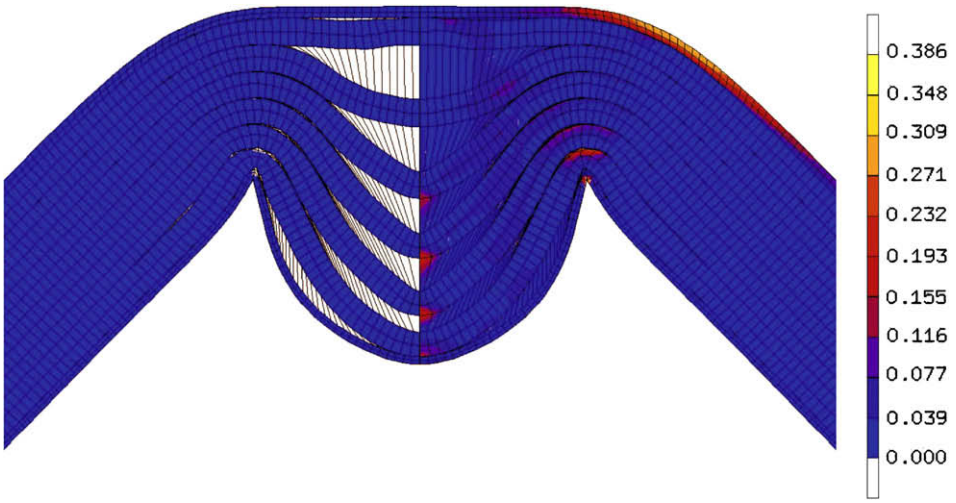

Fig. 16. The computed creasing zone at the end of the folding process; the effective separations (left) and the maximum principal strains (right) are indicated. White zones represent effective separation beyond the traction peak.

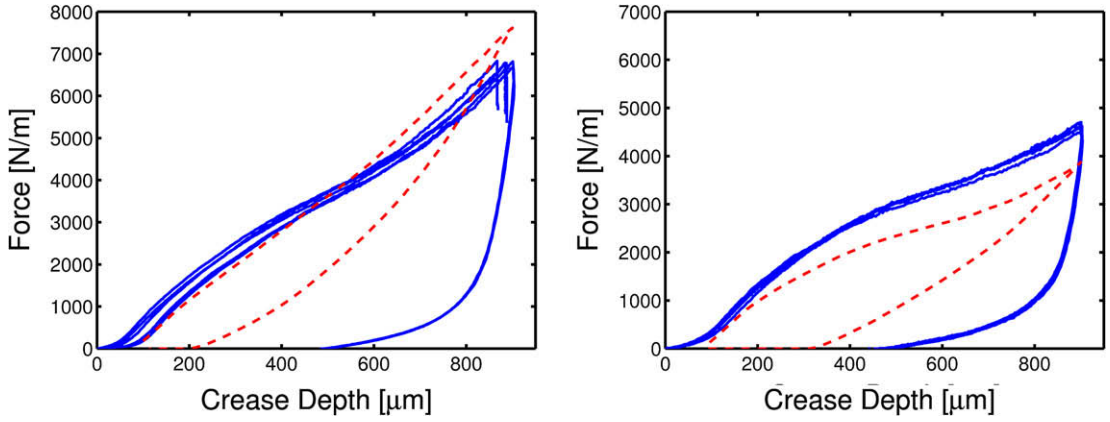

Fig. 17. The experimental (solid) and numerical (dashed) force–crease depth curves for creasing channel widths of 2.25 (left) and 2.75 mm (right).

upper two plies are loaded in in-plane tension while the other plies are loaded in compression and tend to bend inwards.

In the center of the creasing zone no dilation is present between the midlayer and the outer layers in Fig. 16. For the bottom layer this matches the experimental results but between the top layer and the midlayer delamination is clearly visible in the microscopic image in Fig. 3. In the numerical analysis no delamination occurs due to the fact that during creasing these layers are not delaminated below the creasing rule and during folding they are both loaded in in-plane tension, which implies that the out-of-plane normal loading is small. The fact that these layers are separated in the folding experiments may indicate that delamination between the midlayer and the top layer occurs at a lower stress than delamination within the midlayer.

In the right half of Fig. 16 the maximum principal strains are shown to be large in the top layer at the border of the creasing zone, while they are small (less than 1%) in the center. Therefore, the edge of the creasing zone is the location where failure of the top layer would first be expected. However, in the experiments it is not clearly visible where failure occurs due to the heterogeneous structure of the paperboard. Another interesting observation is that the strains are as high as 35% in the numerical results while in the experimental results no failure occurs, although in uniaxial loading in MD the breaking strain of the top layer is only 2%. This suggests that in the folding experiment a complex state of stress is present in the top layer which results in a much higher breaking strain. At the same time, one should realize that the paperboard is modeled here as a laminate of three uniform continua, whereas in reality each layer is highly heterogeneous and surface effects may play an important role.

A discrepancy can be seen between the overall shape of the creasing zone in the experiments and the numerical prediction (see Figs. 3 and 16). In the experiments the lower plies buckle into a rectangular shape due to in-plane compression stresses. However, in Fig. 16 the lower plies show no such buckling. This is caused by the large amount of delamination that occurs between the lower plies in the mechanical model during folding. As a result, the lower plies in the mechanical model can freely bend inwards and no buckling occurs. The lower plies in the experiments are only delaminated at the sides of the creasing zone and not in the center. This results in one thick lower ply in the center which is connected via a number of thin plies to the undeformed paperboard outside the creasing zone (see Fig. 3). The thin plies in the experiments are easy to bend and therefore all bending concentrates in these plies, which ultimately buckle. The thick ply in the middle has a high bending stiffness and remains oriented horizontally. This difference of the shape of the creasing zone however has only a limited effect on the force–crease depth curve.

4.3. Influence of channel width

The force–displacement response is different for different widths of the creasing channel. In Fig. 17 the numerical and experimental force–crease depth curves are presented for channel widths of 2.25 and 2.75 mm, respectively, as opposed to 2.50 mm in the reference case. The initial stiffness of the experimental results, after 125 μm, does not change substantially because mostly the out-of-plane compression zones underneath the creasing rule and above the edge of the creasing channel determine this part of the response. Delamination is initiated in both cases, as can be concluded by the subsequent change of slope. Once the delamination stops, the paperboard is loaded in out-of-plane compression again. Because the contact area of the creasing rule with the board is larger for smaller channel widths, the response is stiffer at the end of the creasing experiment.

The numerical force–crease depth curves for different channel widths deviate somewhat from the experimental data (see Fig. 17). The first part of the numerical response for a width of 2.25 mm fits the experimental results well although no distinctive decrease of slope is present when delamination is initiated. At the crease depth at which delamination stops, the numerical response is stiffer due to the too large out-of-plane stiffness. Interesting is that the numerical response fits the experimental results better than for the wider creasing channels. The cause of this is that for smaller widths out-of-plane shear is less important compared to larger widths. Therefore, delamination, which is initiated by out-of-plane shear, has less influence on the force–crease depth curves and the stiffness deviates less from the initial stiffness when delamination occurs. This is also the reason that the response obtained with a wider creasing channel is lower relative to the response at standard creasing settings. The crease depth at which the delamination stops is larger for a wider creasing channel because the shear zones are larger. Due to this effect the compression-dominated phase starts at a larger crease depth, which contributes to a larger deviation at the end of the creasing test.

Quantitatively the mechanical model predicts paperboard's behavior better for smaller creasing channels (see also Fig. 10). However, qualitatively the numerical results deviate more from the experimental force–crease depth curves for a smaller creasing channel because the decrease of the slope which occurs at about a depth of 200 μm is not correctly predicted. These results show that the way delamination is incorporated in the mechanical model somewhat restricts the use of the model as it overpredicts the trends observed in the experiments.

The experimental and numerical folding results for samples which have been creased with channel widths of 2.25 and 2.75 mm are presented in Fig. 18. The experimental initial stiffness is clearly higher for wider creasing channels. Experimental observations did not show enough detail to reveal the mechanics that are responsible for this trend but two causes are plausible. First the lower plies are less plastically deformed during creasing and secondly it is possible that less delamination has occurred during creasing. Both effects may lead to an increasing stiffness.

The qualitative observation of a higher stiffness for a wider channel in the experimental results is not predicted by the numerical model. The numerical results even show the opposite response which is caused by the overestimated influence of delamination for large channel widths. Due to the relatively large shear zones in which all delamination surfaces open during creasing, the influence of delamination is more pronounced, resulting in a low stiffness of the moment–angle curve. Therefore, the mechanical model cannot be used to explain the trends of the experimental moment–angle curves for different channel widths.

4.4. Influence of crease depth

The experimental creasing results for different crease depths are shown in Fig. 19. The loading curves coincide until the board touches the bottom of the creasing channel at a crease depth of 1450 μm. From this moment onwards the creasing test essentially becomes a compression test and the stiffness increases. Careful inspection of images taken during the tests shows that the average out-of-plane compression strain below the creasing rule is approximately 60% at the moment the board touches the bottom of the channel. The unloading curves show a relatively steeper force decrease for large crease depths.

The right graph in Fig. 19 shows the experimental moment–angle curves for different crease depths. The top solid curve shows the folding result without creasing; the initial bending stiffness equals 0.166 Nm. The sudden drop of the moment observed at 72° is caused by breaking of the top layer. The curve immediately below it is for a crease depth of 500 μm. Although no drop of the moment can be observed, the top layer breaks as well for this crease depth. It is clearly visible that the initial stiffness is higher for smaller crease depths. For a crease depth of 1500 μm no plateau occurs. Crease depths higher than 1500 μm barely lead to any difference in folding behavior because at 1450 μm the paperboard touches the bottom of the creasing channel.

The numerical force–crease depth curves for different crease depths are not presented here because they logically show the same good agreement with the experimental data as in Fig. 10. The experimental folding results for two different crease depths are compared to the numerical results in Fig. 20. The mechanical

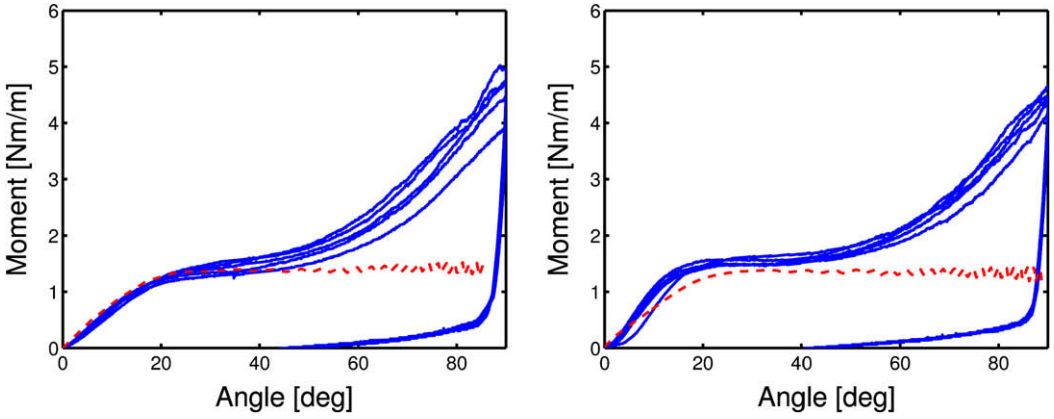

Fig. 18. The experimental (solid) and numerical (dashed) moment–angle curves following creasing with channel widths of 2.25 (left) and 2.75 mm (right).

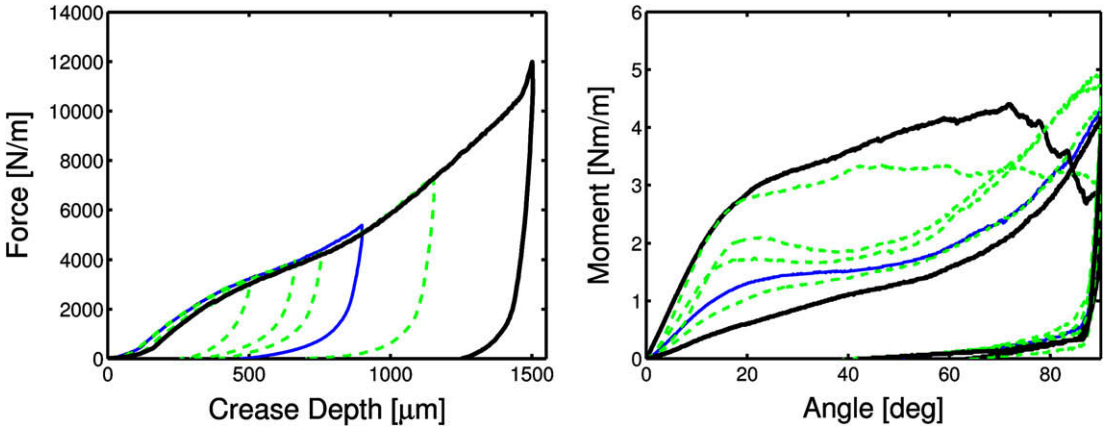

Fig. 19. Experimental force–crease depth curves (left) and corresponding moment–angle curves (right) for different crease depths at otherwise standard creasing settings. The reference case is given by the solid blue/gray curves. The black solid curves are for a crease depth of 1500 μm and an uncreased sample; all the other curves represent intermediate crease depths.

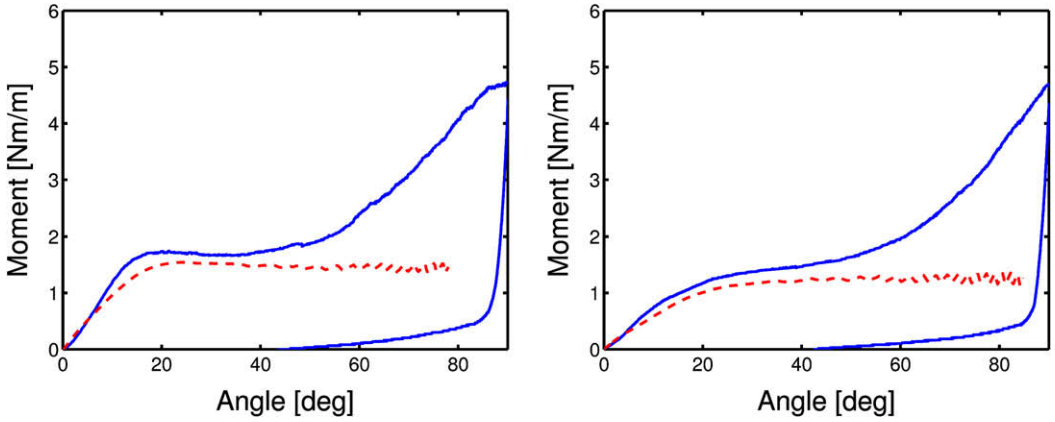

Fig. 20. The experimental (solid) and numerical (dashed) moment–angle curves for crease depths of 750 μm (left) and 1050 μm (right).

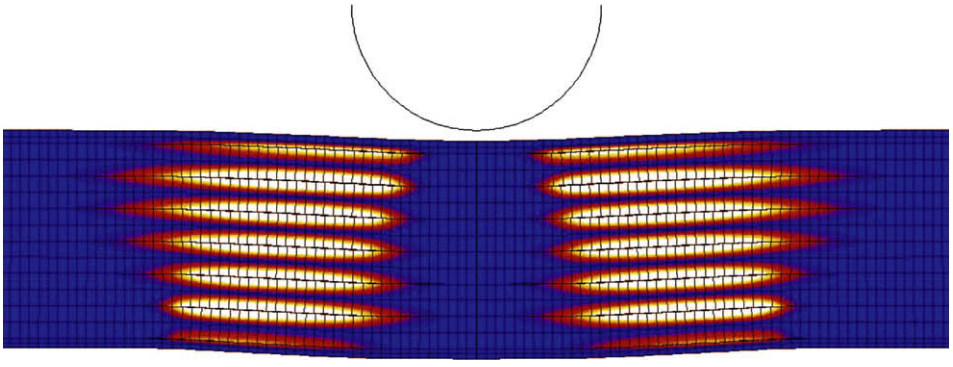

Fig. 21. The computed creasing zone at the end of the creasing process for a crease depth of 500 μm. White zones represent effective separation beyond the traction peak.

model clearly captures the trend of increasing stiffness and increasing plateau level for a decreasing crease depth. The simulation results show that this trend is solely caused by a different amount of plastic deformation in the creasing zone before folding is performed, because the amount of delamination is practically the same in all cases. Moreover, the transition from the initial linear regime to a constant moment is predicted well. However, in both cases the predicted initial stiffness and the plateau moment are slightly smaller compared to the experimental results. This is probably caused by friction due to the aluminum foil between the paperboard and the supports of the bending device, which may be slightly deformed after several tests. Remember that deformation of the aluminum foils is also the cause of the moment increase beyond 40° in the experiments. These observations show that the mechanical model can be used to predict the effect of different creasing depths for the reference width of the channel.

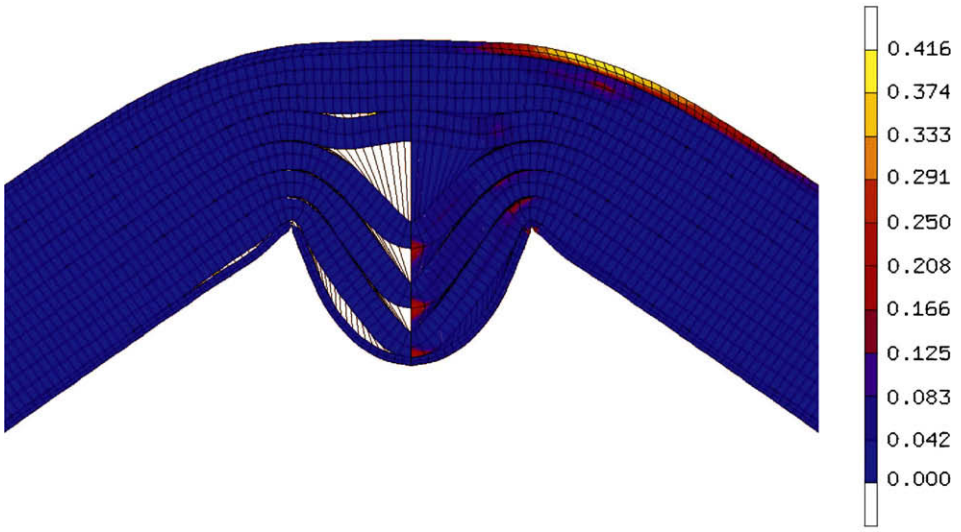

Fig. 22. The computed response during folding at an angle of 72° for a crease depth of 500 μm; the effective separations (left) and the maximum principal strains (right) are shown. White zones represent effective separation beyond the traction peak.

4.5. Failure mechanism for shallow creasing

During the folding test following creasing to a depth of 500 μm or less, the top layer breaks in the experiments. This is an interesting limit because the breaking strain during folding can be deducted from the mechanical model for it. Because in the experimental moment–angle curve it is not clear at which angle the top layer breaks (see Fig. 19), the same angle is assumed at which failure occurs in the folding test with a sample that was not creased at all. The maximum principal strain at this angle is 42%.

Furthermore, these results reveal the mechanics in the creasing zone responsible for breaking. In Fig. 21 the creasing zone is depicted after creasing. Comparing Fig. 21 with the left result in Fig. 15, we see that more or less the same amount of delamination is present in the creasing zone. However, the plastic deformation is much less in Fig. 21 because the board is almost straight. Due to this small amount of plasticity, not all plies can bend inwards during folding, resulting in an increase of the strain in the top layer, which ultimately breaks. This mechanism is illustrated in Fig. 22, which shows the folding response of the shallowly creased board. An important conclusion is therefore that in order to obtain a good crease not only a sufficient amount of delamination must have occurred during creasing but, perhaps more critically, also sufficient plastic deformation.

5. Conclusion

A mechanical model in a finite element framework is proposed to predict and understand the behavior of a three-layer laminated paperboard during creasing and folding. Emphasis is on obtaining a better understanding of the mechanisms that govern both processes, and readily available means are therefore used to keep the model as simple as possible. The structure of the mechanical model and its parameters are based on independent experiments. The model uses an elasto-plastic material description to describe the material behavior of the paper plies. Cohesive zones in combination with Coulomb friction are used to describe the opening behavior of the various plies.

The mechanical model has been validated by force–crease depth curves and strain fields during creasing and moment–angle curves and microscopic images during folding. Although the computed moment–angle curves match the experimental data quite well, substantial differences sometimes occur between the predicted and the experimentally observed local deformation. It is therefore questionable if moment–angle curves, which are routinely used in the industry, are a meaningful predictor of the quality of a crease.

For the standard creasing settings and small deviations from them, the mechanical model describes the paperboard's behavior during creasing and folding well. The accuracy of the predicted force–crease depth curves is limited by the linear elastic modeling of the out-of-plane compression response. Furthermore, the way in which delamination is incorporated leads to comparatively poor predictions for both small and large channel widths.

The mechanical model predicts that high maximum principal strains occur in the top layer at the border of the creasing zone. This indicates that the top layer is most likely to fail at that point. The strain reached here during folding is much higher than in uniaxial loading cases. This suggests that a complex state of stress influences the breaking strain of paper. In future research, a failure criterion that takes this observation into account may be incorporated in the material model. Moreover, in future research the samples must be clamped during creasing because this more accurately resembles an industrial creasing process.

An important conclusion reached using the proposed mechanical model is that not only delamination is necessary to obtain a good crease (as is well-known in the paperboard literature and industry) but also a sufficient amount of plastic deformation must have occurred during creasing. The mechanical model has also exposed the failure mechanism that operates if no plastic deformation has occurred, such as in the case of shallow creasing. Some of the plies which are normally expected to bend away then remain straight, resulting in a more severe stretching of the top layer. The folding results of Nagasawa et al. (2003) indicate that the same mechanisms are probably active during creasing and folding of thin paperboards. It therefore seems likely that for thin boards plastic deformation is also essential to obtain a good crease.

The mechanical model uses a somewhat simple material and delamination description but nevertheless the mechanics that operate during paperboard creasing and folding are adequately described. One improvement may be achieved by modeling the paperboard's out-of-plane compression response as non-linear elasto-plastic instead of linear elastic. However, this modification would merely improve the predicted force–crease depth curve,

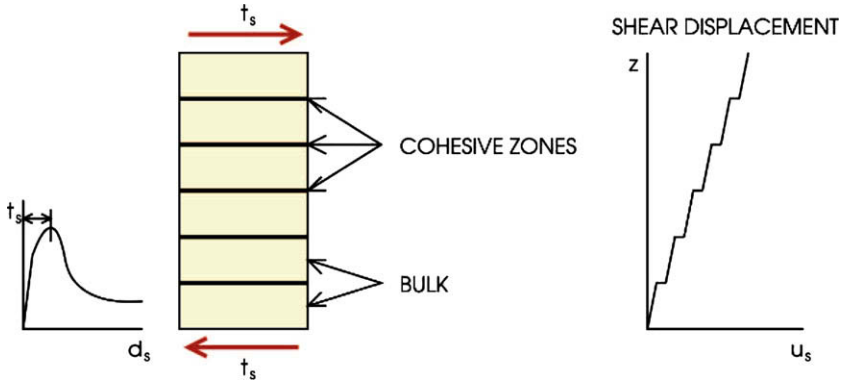

Fig. 23. Schematic representation of the mechanics in the idealized midlayer before the maximum shear stress is reached. The bulk and the five cohesive zones all contribute to the total displacement. This leads to the displacement distribution u_s which is shown as a function of the thickness coordinate.

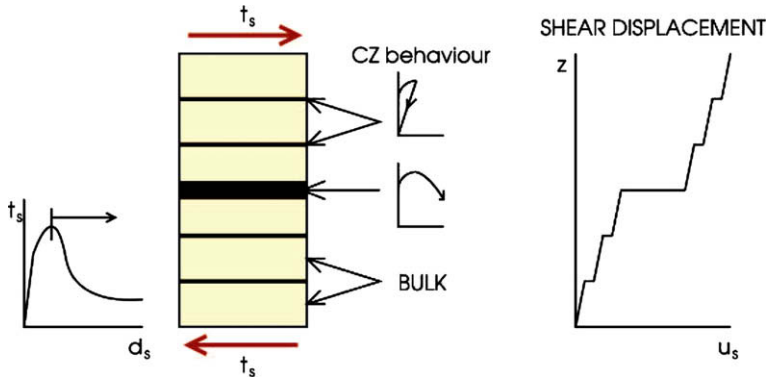

Fig. 24. Schematic representation of the mechanics in the idealized midlayer after the maximum shear stress is reached. The relative displacement of a single cohesive zone (thick line) increases while the other cohesive zones unload. This is clearly visible in the graph, where the displacement u_s is shown as a function of the thickness coordinate.

which in practice is of little interest. A more significant improvement may result for a less idealized modeling of the delamination, for example by a distribution of delamination strengths. However, whether the added experimental identification burden necessary for this change is worthwhile remains to be seen.

Acknowledgements

The comments and paperboard provided by Mayr-Melnhof Eerbeek are gratefully acknowledged by the authors. They also thank Marc van Maris for his enthusiastic support in the experimental work.

Appendix A. Experimental characterization of a cohesive zone

Out-of-plane shear experiments in MD are performed to characterize the traction–separation law of one cohesive zone. In the mechanical model of paperboard as sketched in Fig. 5 seven cohesive zones are present across the thickness of the board, of which two are in between the midlayer and the outer layers and five within the midlayer. The shear tests have been performed solely on the midlayer and thus correspond with a model consisting of the bulk material and five cohesive zones loaded in series.

Before the maximum shear stress of the cohesive zones is reached, the total tangential displacement consists of the displacement of the six bulk plies plus the relative displacement of the five identical cohesive zones (see Fig. 23). To extract the response of a cohesive zone, the results must therefore first be corrected by subtracting the shear of the bulk. This response is formulated as follows:

$$u_b = h\frac{t_s}{G_{13}}, \tag{9}$$

where t_s is the shear stress, G_{13} represents the out-of-plane shear modulus in MD, u_b represents the total tangential displacement due to the bulk and h is the thickness of the midlayer. The resulting shear displacement $u_s - u_b$, before the maximum shear stress is reached, must now be divided by five as the five cohesive zones show the same relative displacement (see Fig. 23).

A different situation occurs beyond the maximum shear stress. Post-peak, the displacement of one cohesive zone in the model continues to grow while the other four unload according to the secant stiffness predicted by the damage formulation of the cohesive zone model (see Fig. 24). The post-peak response of a single cohesive zone is therefore obtained by subtracting the elastic response of the bulk as well as that of the four remaining cohesive zones from the measured shear response.

In both cases the cohesive zone response obtained is in terms of $t_s = \beta\tau$ and $\delta_s = \lambda/\beta$ and must thus be scaled by β to obtain $\tau(\lambda)$. The final result is shown in Fig. 8.

References

Barbier, C., Larsson, P.L., Östlund, S., 2004. On dynamic effects at folding of coated papers. Composite Structures 67, 395–402.

Beldie, L., 2001. Mechanics of paperboard packages – performance at short term static loading, Licentiate Dissertation. Lund University, Lund, Sweden.

Beex, L.A.A., 2008. Experimental and computational study of laminated paperboard creasing and folding. Master's thesis. Eindhoven University of Technology, Eindhoven, The Netherlands.

Castro, J., Ostoja-Starzewski, M., 2003. Elasto-plasticity of paper. International Journal of Plasticity 19, 2093–2098.

Chandra, N., Li, H., Shet, C., Ghonem, H., 2002. Some issues in the application of cohesive zone models for metal–ceramic interfaces. International Journal of Solids and Structures 39, 2827–2855.

Choi, D.D., Lavrykov, S.A., Ramarao, B.V., 2007. Simulation studies of delamination effects in the scoring and folding of paperboard. In: Proceedings: 61st Appita Annual Conference and Exhibition, Gold Coast, Australia, 6–9 April 2006. Carlton, Vic., Appita Inc., pp. 209–216.

Hill, R., 1950. Mathematical Theory of Plasticity. Cardon Press, Oxford, United Kingdom.

Isaksson, P., Hägglund, R., Gradin, P., 2004. Continuum damage mechanics applied to paper. International Journal of Solids and Structures 41, 4731–4755.

Isaksson, P., Hägglund, R., 2005. A mechanical model of damage and delamination of corrugated board during folding. Engineering Fracture Mechanics 72, 2299–2315.

Karafillis, A.P., Boyce, M.C., 1993. A general anisotropic yield criterion using bounds and a transformation weighting tensor. Journal of the Mechanics and Physics of Solids 41, 1859–1882.

Mäkelä, P., Östlund, S., 2003. Orthotropic elastic–plastic material model for paper materials. International Journal of Solids and Structures 40, 5599–5620.

Nagasawa, S., Fukuzawa, Y., Yamaguchi, T., Tsukatani, S., Katayami, I., 2003. Effect of crease depth and crease deviation on folding deformation characteristics of coated paperboard. Journal of Materials Processing Technology 140, 157–162.

Ortiz, M., Pandolfi, A., 1999. Finite-deformation irreversible cohesive elements for three-dimensional crack-propagation analysis. International Journal of Numerical Methods in Engineering 44, 1267–1282.

Ramberg, W., Osgood, W.R., 1943. Description of Stress–Strain Curves by Three Parameters, Technical Note No. 902, NACA (National Advisory Committee for Aeronautics).

Savolainen, A., 1998. Paper and Paperboard Converting, Finnish Paper Engineers' Association. Fapet Oy, Jyväskylä, Finland.

Sawyer, J.P.G., Jones, R., MacKinlay, P.R., 1998. A unified constitutive theory for paper. Composite Structures 42, 93–100.

Stenberg, N., 2003. A model for the through-thickness elastic–plastic material behaviour of paper. International Journal of Solids and Structures 40, 7483–7498.

Thakkar, B.K., Gooren, L.G.J., Peerlings, R.H.J., Geers, M.G.D., 2008. Experimental and numerical investigation of creasing in corrugated paperboard. Philosophical Magazine 88, 3299–3310.

Van den Bosch, M.J., Schreurs, P.J.G., Geers, M.G.D., 2007. A cohesive zone model for with a large deformation formulation accounting for interfacial fibrilation. European Journal of Mechanics A/Solids 26, 1–19.

Van Hal, B.A.E., Peerlings, R.H.J., Geers, M.G.D., Sluis van der, O., 2007. Cohesive zone modeling for structural integrity analysis of IC interconnects. Microelectronics Reliability 47, 1251–1261.

Xia, Q.S., Boyce, M.C., Parks, D.M., 2002. A constitutive model for the anisotropic elastic–plastic deformation of paper and paperboard. International Journal of Solids and Structures 39, 4053–4071.

Xia, Q.S., 2002. Mechanics of inelastic deformation and delamination in paperboard, Ph.D. thesis. Massachusetts Institute of Technology, Massachusetts, United States of America.

Xu, X.P., Needleman, A., 1993. Void nucleation by inclusion debonding in a crystal matrix. Modelling and Simulation in Materials Science and Engineering 1, 111–132.